JOURNAL OF MATERIALS SCIENCE 14 (1979) 287–295

Stress relaxation in coiled ribbons of $Fe_{40}Ni_{40}P_{14}B_6$ and $Fe_{29}Ni_{49}P_{14}B_6S_2$

D. G. AST, D. J. KRENITSKY
Department of Materials Science and Engineering, Cornell University, Ithaca, New York 14853, USA

The stress relaxation at elevated temperatures in coiled ribbons of Fe-Ni base metallic glasses is calculated for both power law creep and Eyring activated flow. The results are compared with experimental data on the spring-back of coiled ribbons after various anneals. Good agreement is obtained for Eyring activated flow, but not for power law creep. Comparison with stress relaxation experiments on straight sections indicates that stress relaxation in coiled ribbons is largely due to transient creep.

1. Introduction

The tensile compliance of metallic glasses consists of three contributions: (a) an instantaneous elastic part, (b) a transient or anelastic part and (c) a steady state or plastic part [1]. The transient part is largely, but not completely recoverable. The non-recoverable fraction of the transient compliance is on the order of 5% or less [2], and is ascribed to the relaxation of the quenched glass towards a more stable structure [2]. This contribution therefore decreases with the number of test cycles on a given specimen [2].

The relative magnitude of the three contributions to the tensile compliance varies with temperature. At high temperatures ($T_g > T > T_g - 20^\circ$ C) the anelastic contribution becomes very large – about 200 times larger than the elastic contribution. In this narrow temperature range, metallic glasses behave therefore almost like glassy polymers. Sufficiently below T_g, the anelastic contribution is of the order of the instantaneous elastic contributions, or fractions thereof.

According to [2] the nature of the anelastic element at low temperatures ($T_g - 110 < T < T_g - 210^\circ$ C) and low stresses is Maxwellian, but at stresses higher than about a quarter of the yield stress a more complex behaviour is observed [2]. Recently a more detailed analysis has shown that in Pd–Si glasses the recoverable (i.e. majority) and non-recoverable (minority) part of the transient component can be modelled with a Maxwell element in series with a Voight element [3].

The steady state or plastic deformation is viscous only at high temperatures ($T_g - 30 < T < T_g$) where it follows the Vogel–Fulcher equation. Below this range, the temperature dependence of the plastic flow is usually expressed by an Arrhenius expression with a temperature dependent activation energy. The activation energy decreases rapidly below $T_g - 30^\circ$ C and reaches an approximately constant value in the region where the viscosity is greater than about 10^{15} N m^{-2} sec. In the region $T_g - 210 < T < T_g - 110^\circ$ C the measured activation energy for Pd–Si based metallic glasses is 0.5 eV [2], and 0.1 to 1 eV in Ni–P or Co–P based metallic glasses [4].

The stress dependence of the plastic deformation is small and can, within the experimental error, be satisfactorily described by both an Erying model and by a power law [2]. The Eyring model yields an activation volume v^* of the order of an atomic volume Ω [1, 2]. Alternatively, the power law description $\dot{\epsilon} = A\sigma^n$, fits the data with $n = 1.6$ in Pd base glasses [2] and 1 in Ni–P [3]. For temperatures closer than about 10° C to T_g, the stress dependence increases rapidly and v^* may reach 100 Ω [1].

Most of the reported mechanical data on amorphous alloys pertain to Pd–Si based metallic glasses which can be prepared more easily than the

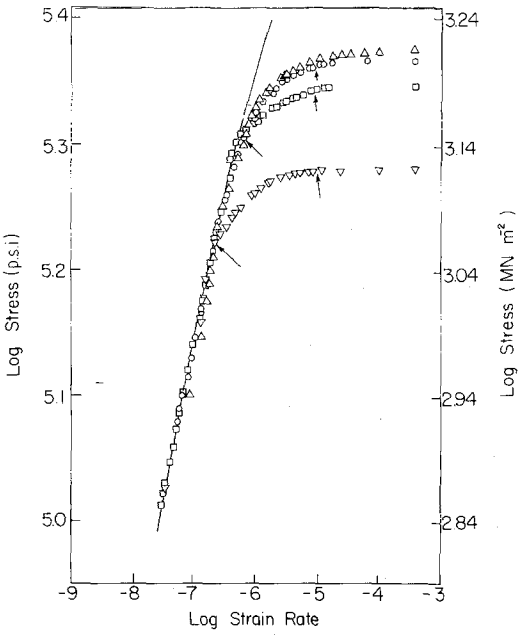

Figure 1 Log_{10} of stress versus $\log_{10}$ of strain rate as measured in a tensile test stress relaxation experiment. Results are shown for four different initial load levels. Test temperature is 270° C. The specimen was pre-annealed at 300° C to stabilize the structure.

Ni–Fe based variety. In view of this situation we studied the relaxation behaviour of Ni–Fe base metallic glasses in considerable detail [5]. This paper reports an analysis of the transient deformation which, as we will show, dominates the stress relief in practical annealing situations such as is encountered in the annealing of wound transformer cores.

2. Experimental

Two types of experimental data are available for an analysis of the stress relaxation behaviour of amorphous $Fe_{40}Ni_{40}P_{14}B_6$ (Tradename Allied Metglas #2826). These are stress relaxation data from tensile tests [5] and spring-back measurements on 2826 ribbons coiled into rings prior to anneal [6, 7].

A typical result of a stress relaxation test under tension is shown in Fig. 1, which illustrates the relation between stress (vertical axis) and strain rate (horizontal axis) for four different initial stress levels. It can be seen that the $\log_{10}\sigma$ versus $\log_{10}\dot{\epsilon}$ relation consists phenomenologically of three parts, the borders between which are indicated by arrows in Fig. 1. Part 1 commences immediately after termination of loading and is characterized by an extreme sensitivity of the strain rate to stress. At 270° C, this part is completed in about 60 sec. Part 2 is the transient or anelastic deformation, which eventually merges into part 3, the steady state or plastic deformation. The transition between parts 2 and 3 is gradual and at 270° C occurs around 5 h, give or take a factor of 2. Part 3, the steady state deformation, is very accurately described by a power law with a stress exponent of about 4. A detailed investigation reveals that the stress exponent of a well annealed sample ($T_{\text{anneal}} = 300°$ C) tested repeatedly at 270° C changes slightly with the number of load cycles rising from about 3.7 after the first loading to about 4.3 after the 6th loading. These changes are too small to be detected in Fig. 1 and are therefore shown separately in Fig. 2.

As the temperature is lowered, the time to reach steady state deformation increases very rapidly so that for practical time intervals this section of the log σ versus log $\dot{\epsilon}$ curve soon becomes unobservable.

Tests on ribbons coiled into rings prior to anneal are easily carried out and a number of investigators have used these tests as a qualitative means to check stress relief in wound ribbons. The most detailed measurements, by far, are those by Graham *et al.* [6], whose measurements are reproduced in Figs. 3, 4 and 5. Their specimens were coiled into rings of 6.5 mm prior to anneal at various temperatures and times. After each anneal,

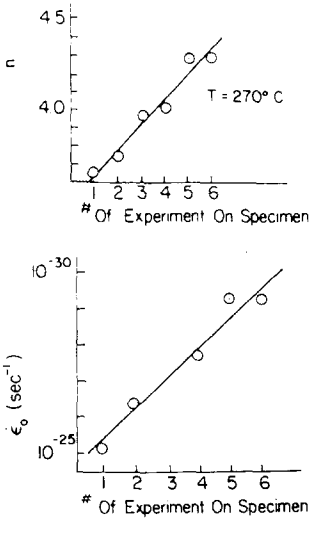

Figure 2 Stress exponent and pre-exponential factor as measured in repeated tensile test stress relaxation experiments on one specimen. Test temperature is 270° C.

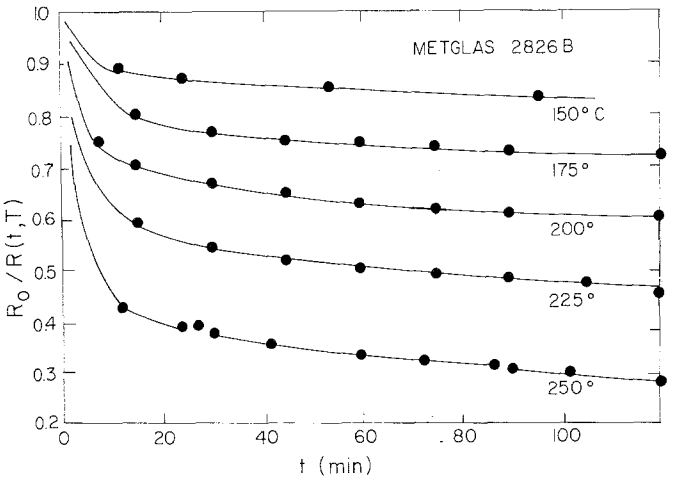

Figure 3 Short term annealing behaviour of 2826B measured from the spring-back of coiled ribbons. Data from [6].

the equilibrium radius of curvature was measured. Stress relaxation was then plotted on a scale from 1, corresponding to the initial stress, to 0, corresponding to complete stress relaxation or zero spring-back. These investigators reported that they tried unsuccessfully to deduce activation energies from the data, or to fit the curves to conventional kinetic equations

In the following section we will analyse their data and show that they can be accounted for by an Eyring type flow.

3. Analysis

The task at hand is to evaluate the time dependent stress distribution in the ribbon, as progressive relaxation changes the initial linear elastic stress distribution introduced by coiling at the time $t = 0$. Out of the many models proposed for relaxation, two flow laws were investigated in detail in this analysis. The respective laws were an Eyring activated state model:

$$\dot{\epsilon} = \dot{\epsilon}_0 \exp(-\Delta H/kT) \sinh(v^* \sigma/kT) \quad (1)$$

and a power law of the form:

$$\dot{\epsilon} = \dot{\epsilon}_0 \exp(-\Delta H/kT)(\sigma/\sigma_0)^n \quad (2)$$

If the stress distribution $\sigma(z, t)$ is known, the stress distribution at the time $t + \Delta t$, is given by

$$\sigma(z, t + \Delta t) = \sigma(z, t) - E \cdot \dot{\epsilon}(z, t) \cdot \Delta t \quad (3)$$

where E is the elastic modulus (Young's modulus). For $\Delta t \to 0$, one obtains with flow laws 1 and 2.

$$\frac{\partial \sigma}{\partial t} = -2E\dot{\epsilon}_0 \exp(\Delta H/kT) \sinh(v^* \sigma/kT) \quad (4)$$

and

$$\frac{\partial \sigma}{\partial t} = -E\dot{\epsilon}_0 (\sigma/\sigma_0)^n \exp(-\Delta H/kT) \quad (5)$$

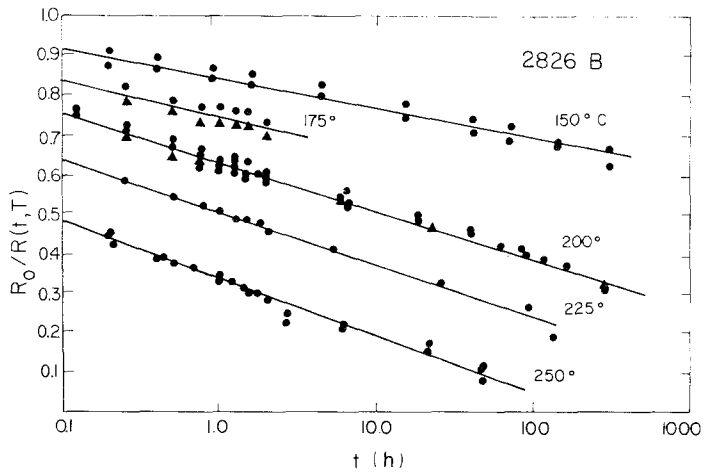

Figure 4 Long term annealing behaviour of 2826B measured from the spring-back of coiled ribbons. Data from [6].

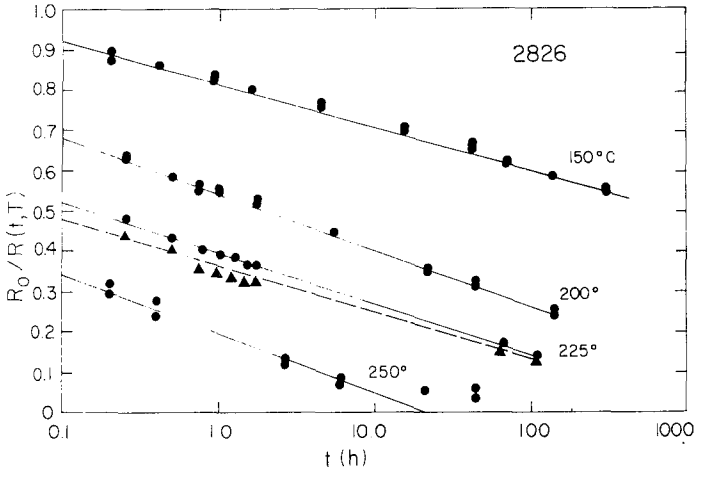

Figure 5 Long term annealing behaviour of 2826 measured from the spring-back of coiled ribbons. Data from [6].

The boundary condition is that for $t = 0$ the stress distribution is linear, i.e.

$$\sigma(z, 0) = (2z/d)\sigma_0$$

where z is the coordinate perpendicular to the plane of the ribbon starting at the neutral axis, d the thickness of the ribbon and σ_0 the elastic surface stress at $t = 0$. The general solution of Equation 4 is given by.

$$\frac{\sigma}{\sigma_0} = \frac{kT}{v^*\sigma_0} \ln \frac{1 + f(z)f(t)}{1 - f(z)f(t)} \tag{6}$$

where

$$f(t) = \exp\left[-E\dot{\epsilon}_0 \exp(-\Delta H/kT)v^*/kT\right]$$

and

$$f(z) = \frac{\exp\left[\sigma(z, 0)v^*/kT\right] - 1}{\exp\left[\sigma(z, 0)v^*/kT\right] + 1}$$

With the help of hyperbolic functions Equation can be concisely as:

$$(\sigma/\sigma_0) = (kT/v^*\sigma_0)\, 2 \operatorname{arctanh}\{\tanh[\sigma(z, 0)/2kT] \exp[-2E\dot{\epsilon}_0 \exp(-\Delta H/kT)v^*/kT]\} \tag{7}$$

The solution for power law creep is simpler and given by:

$$(\sigma/\sigma_0) = \left[1 - \frac{E\dot{\epsilon}_0 \exp(-\Delta H/kT)(n-1)t}{\sigma_0^n \sigma(z, 0)^{1-n}}\right]^{1/(1-n)} \tag{8}$$

These equations have been evaluated with the aid of a PDP 12 computer and Figs. 6 and 7 show calculated stress distributions in coiled ribbons at various times for the two flow laws. The values chosen for the flow parameters, $v^* = 400\ \text{Å}^3$ and $n = 13$ are typical for what one obtains from an analysis of experimental data. The general behaviour in Figs. 6 and 7 is quite similar except at

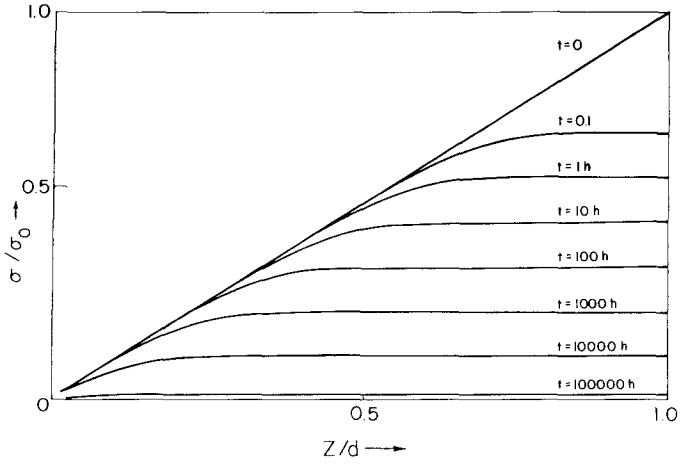

Figure 6 Calculated time dependent stress distribution in the ribbon, measured from the neutral axis. The calculation assumes that transient creep follows a hyperbolic flow law with $v^* = 400\ \text{Å}^3$.

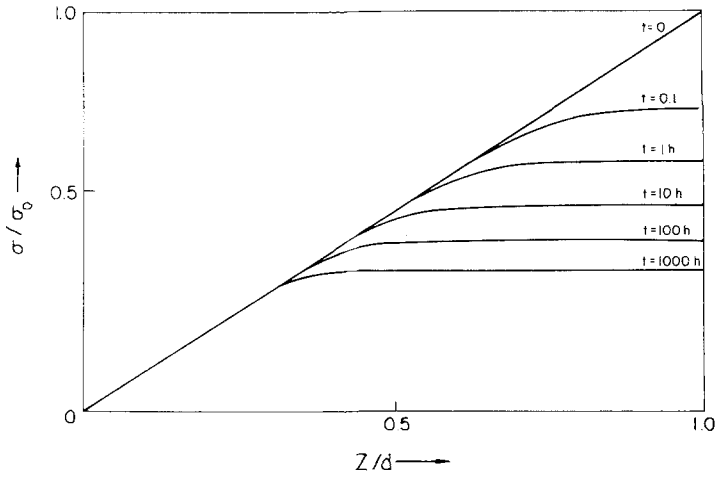

Figure 7 Calculated time dependent stress distribution in the ribbon measured from the neutral axis. The calculation assumes that transient creep follows a power law with $n = 13$.

low stresses where the power law gives a much slower stress relief with time. This behaviour generates, as we will see, a "tail" in the time dependent moment which is characteristic for power law creep.

The stress distributions 7 and 8 can be used to calculate the time dependent moments which are directly related to the observed radii of curvature:

$$M(t)/M(t_0) = \int_0^{d/2} \sigma(z,t)z\,dz \Big/ \int_0^{d/2} \sigma(z,0)z\,dz \tag{9}$$

This integration was carried out numerically on a PDP 12 computer, except for the case $n = 4$ which can be integrated easily in closed form, yielding:

$$M(t)/M(t_0) = (3/2\phi)[(1+\phi)^{2/3} - 1] \tag{10}$$

with

$$\phi = [3E\dot{\epsilon}_0 \exp(-\Delta H/kT)] \cdot [t/\sigma_0]$$

σ_0 is given by the geometry. The other parameters i.e $\dot{\epsilon}_0$, ΔH, and v^* or, alternatively n, which enter Equation 9 were varied in an attempt to match

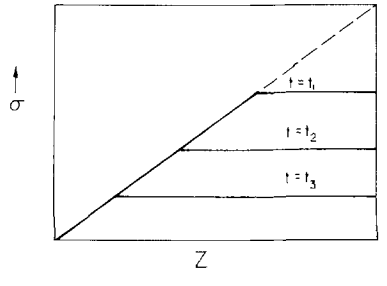

Figure 8 Approximation used for the closed solution of Equation 11 for $M(t)/M(0)$.

the experimental data. In the initial stage of parameter fitting, we found it convenient to approximate the actual stress distribution with two linear sections (see Fig. 8). The moment is then simply given by:

$$M(t)/M_0 = (1.5 \cdot \sigma(d/2,t) - (0.5 \cdot \sigma(d,t)^3) \tag{11}$$

where $\sigma(d/2, t)$ is given by Equations 7 and 8 respectively. The approximation is fairly accurate even for moderate stress dependence ($n = 4$, see Figs. 9 and 10) and becomes quite accurate at higher stress dependences ($n = 13$) where the deviations between the actual and the approximate stress dependence become small.

4. Results

Comparisons between the results of the calculations and the experimental data are shown in Figs. 9 to 14.

It was found that the stress relief in coiled ribbons could not be described with a power type flow law. Figs 9 and 10 show the best fit obtained for $n = 4$; i.e. the flow law which describes the steady state or plastic deformation part of the stress relaxation curve of Fig. 1. The calculated curves fall faster with the time than experimentally observed, indicating the stress relaxation in coiled ribbons is not caused by plastic flow. Treating n as an adjustable parameter did not improve the fit. A typical result is shown in Fig. 11. The choice of $n = 13$ generates a good fit for the 150° C annealing data, but fails to represent the slope of the experimental data at other annealing temperatures. In addition one finds that the shift of the annealing

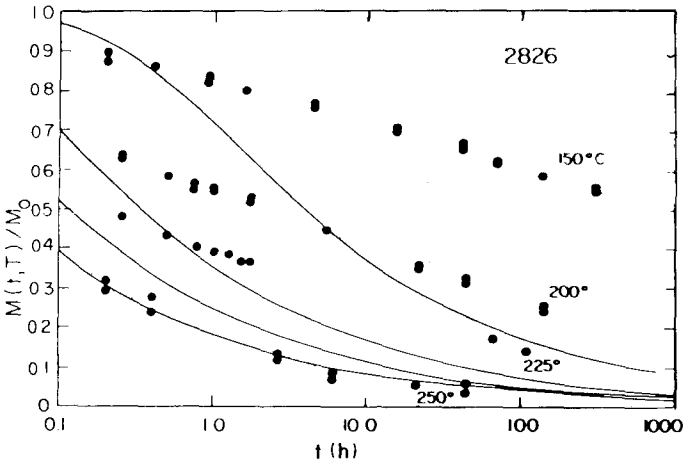

Figure 9 Stress relief in coiled ribbons, assuming a power law with $n = 4$ for transient creep. Solid lines are calculated, using the approximation indicated in Fig. 8. Dashed lines connect experimental results.

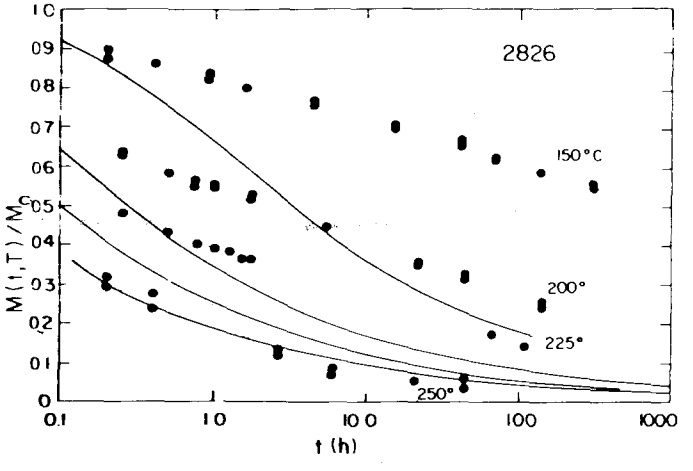

Figure 10 Stress relief in coiled ribbons, assuming a power law with $n = 4$ for transient creep. Solid lines are calculated numerically. Dashed lines connect experimental results.

curves with temperature can not be described with a single activation energy.

The results obtained with an Eyring type hyperbolic flow law are depicted in Figs. 12 to 14, which show both the results obtained with 2826 (composition $Fe_{40}Ni_{40}P_{14}B_6$) and with 2826B (composition $Fe_{29}Ni_{49}P_{14}B_6Si_2$).

Fig. 12 shows that the long term ($0.1 < t < 1000$ h) annealing of coiled 2826B ribbons can be matched successfully with such a flow law. The parameters entering the calculation were $\dot{\epsilon}_0 = 9 \times 10^{18}\ h^{-1}$; $\Delta H = 2.46$ eV (56.6 kcal mol^{-1}); and $v^* = 400\ Å^3$. The accuracy with which these parameters can be determined is about 10% in the

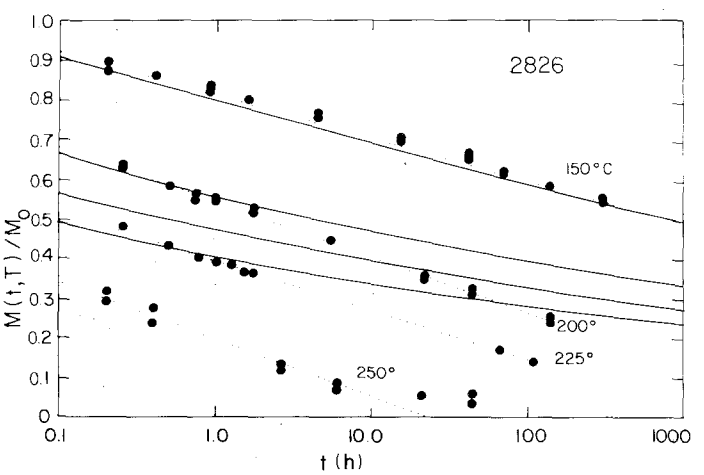

Figure 11 Stress relief in coiled ribbons, assuming a power law with $n = 13$ for transient creep. Solid lines are calculated numerically. Dashed lines connect experimental results.

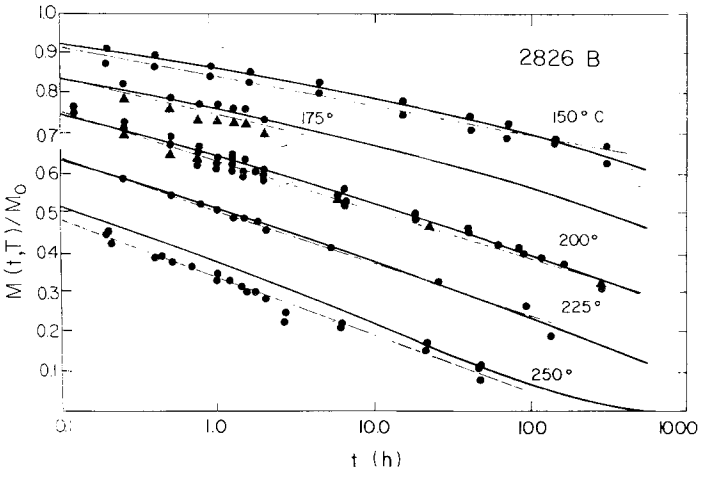

Figure 12 Stress relief in coiled ribbons, assuming a hyperbolic flow law with $v^* = 400\,Å^3$, $\Delta H = 2.46\,eV$, $\dot{\epsilon}_0 = 9 \times 10^{18}$ for transient creep. Long term behaviour. Solid lines are calculated numerically. Dashed lines connect experimental results.

case of $\dot{\epsilon}_0$ and 5% or better in the case of ΔH and v^*. Besides a good overall matching, the calculated curves reproduce previously unnoticed trends in the experimental data such as a slight negative curvature of the annealing curves at lower annealing temperatures. The slight deviation in the position (but not the slope) of the 250° C isotherm is probably a real effect and will be discussed later.

The predictions for the short term annealing behaviour of 2826B, using the *same* set of parameters, is shown in Fig. 13. The good agreement between theory and experiment indicates that the same process that controls the long term annealing behaviour also controls the short term annealing behaviour down to ~7 min, i.e. the shortest annealing times studied.

Next, we present the results obtained on 2826. Fig. 14 shows that very good fits can be obtained for $T = 150$ and 200° C, but that for $T = 225$ and $T = 250$° C deviations set in at longer annealing times. There are not enough experimental data to fix the onset of these deviations reliably for $T = 225$° C. At 250° C, the deviations set in somewhere between 5.6 h (the last data point fitted by the theoretical prediction) and 45 h (the first data point to show an unambiguous deviation). The direction of the deviations are towards larger times; i.e. annealing proceeds slower than predicted. The values entered for 2826 were $\dot{\epsilon}_0 = 6 \times 10^{19}$; $\Delta H = 2.414\,eV$ (55.6 kcal); and $v^* = 360\,Å^3$.

5. Discussion

The deviations observed in 2826 annealed for long times at high temperatures are easily understood with the aid of Fig. 1 which shows that after several hours time, transient creep is replaced by steady state creep (the exact time at which this transition occurs is stress dependent and for this

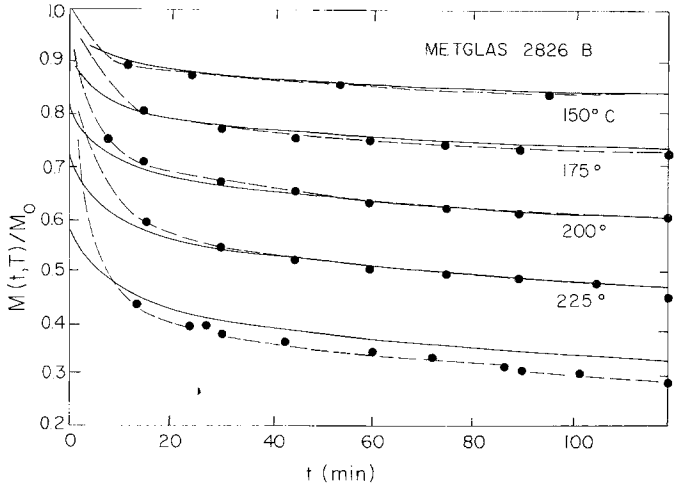

Figure 13 Stress relief in coiled ribbons, assuming a hyperbolic flow law with $v^* = 400\,Å^3$, $\Delta H = 2.46\,eV$, $\dot{\epsilon}_0 = 9 \times 10^{18}$ for transient creep. Short term behaviour. Solid lines are calculated numerically. Dashed lines connect experimental results.

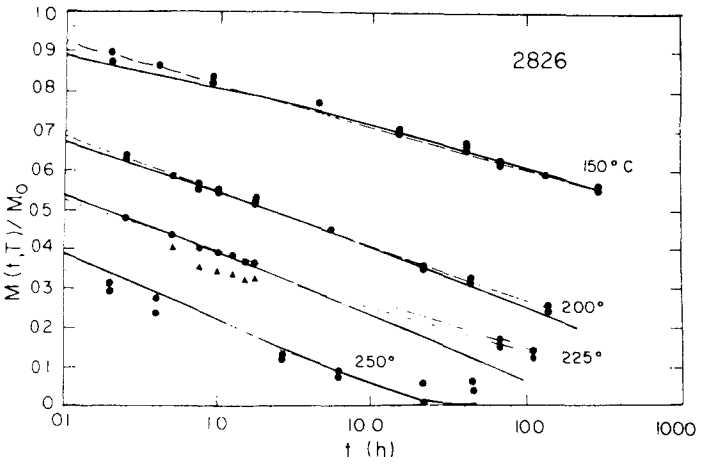

Figure 14 Stress relief in coiled ribbons, assuming a hyperbolic flow law with $v^* = 360\,\text{Å}^3$, $\Delta H = 2.41\,\text{eV}$, $\dot{\epsilon}_0 = 6 \times 10^{19}$ for transient creep. Long term behaviour. Solid lines are calculated numerically. Dashed lines connect experimental results.

reason the two sets of data can not be compared directly). Extrapolation of the transient creep equation to low stress levels results in an overestimate of the creep rate which accounts for the observed deviations. It would be desirable to have more accurate stress relaxation data on coiled ribbons at high temperatures and long annealing times to confirm this interpretation by a direct analysis of the experimental data along the lines of Equation 7.

The results on both plastic or steady state and the transient or anelastic creep in Fe–Ni based metallic glasses are somewhat surprising. In the plastic range, the very high precision of the stress relaxation data allows an experimental discrimination between a power law description and a hyperbolic flow model. Such an analysis shows that a power law with $n \sim 4$ fits the experimental data within the small experimental errors whereas a hyperbolic fit results in small but systematic deviations just outside the experimental scatter. (If one nevertheless analyses such a fit one finds v^* for steady state creep of the order of an atomic volume which agrees with the observation on Pd–Si based glasses). The stress exponent of ~ 4, is unusual in view of the results on both Pd–Si based glasses ($n = 1.6$) and Ni–P ($n = 1$). It also does not agree with the prediction of the free volume theory which predicts $n = 1$ [8]. Dislocation models, of course, can easily account for the observed steady state creep exponent.

In the transient or anelastic deformation, considerable rearrangement must be involved on an atomic scale, as indicated by the large activation volume (~ 20 atomic volumes). The good matching of the calculated and experimental slopes at all temperatures indicate that v^* does not depend on temperature in the temperature range investigated.

The activation energy for transient creep of ~ 2.4 eV appears high compared to the reported activation energy for steady state creep in Fe–Ni base alloys ($Q = 0.35$ eV in Ni–P), but matches, as is to be expected, those measured for internal friction (2.2 to 2.6 eV). The deviation between calculation and experiment observed at 250° C in 2826 B (but not in 2826) could indicate a shift to higher activation energies as T approaches T_g. Such shifts are commonly observed in polymers if $T > T_g - 30°$ C. It is conceivable that the large structural instability of metallic glasses, relative to polymers, gives rise to such effects at temperatures which are in the order of $T_g - 100°$ C. To settle this question conclusively, data at higher annealing temperatures are needed. At the moment, the only activation energy available for the high temperature behaviour of 2826 is the activation energy of crystallization (3.9 eV [9] at 400° C).

The activation energy for transient creep of 2826 B is about 0.05 eV higher than that of 2826, a difference which is likely within experimental error. The trend, however, follows the observation on the activation energies for crystallization which increases with the number of atomic species in the alloy [9].

By replotting the transient portion of Fig. 1 in a suitable coordinate system, one can show in an independent way that the anelastic relaxation follows roughly a hyperbolic flow law with a v^* of about $400\,\text{Å}^3$.

The maximum, initial stress levels in the coiled ribbons investigated here are only about 1/3 of the initial stress levels in the tensile relaxation

specimen of Fig. 1 so that a direct comparison of the relaxation behaviour cannot be carried out.

This is illustrated by the pre-exponential factor in the transient creep equation which depends on the initial loading in the specimen. The reasons for this can be seen from Fig. 1 which shows relaxation of 2826 in a tensile arrangement at four different load levels. The transients are quite similar, i.e. relaxation follows the same basic flow law. However, the stress relaxation at a lower load level does not fall on the extension of stress relaxation initiated at a higher stress level. Rather the translation at different load levels occurs along a line which approximately parallels the steady state creep curve. The pre-exponential factor $\dot{\epsilon}_0$ therefore changes with stress in an approximately power-like fashion, with a stress exponent of 4 if σ is normalized relative to σ_0.

6. Summary

The stress relaxation process in coiled ribbons of Fe–Ni based metallic glasses has been analysed.

It is found that the stress relaxation is almost entirely due to transient, non-steady state, deformation which follows a hyperbolic flow law. The activation energies are 2.41 eV for 2826 and 2.46 eV for 2826 B. The activation volumes are 360 $Å^3$ in 2826 and 400 $Å^3$ in 2826 B.

Steady state creep is only reached after very long anneals at high temperatures and at stress levels of 10% or less of the initial stress level.

Acknowledgements

This research was supported by the Office of Naval Research under Contract NR039-151 and by the Material Science Center at Cornell.

References

1. H. S. CHEN and M. GOLDSTEIN, *J. Appl. Phys.* **43** (1972) 1642.
2. R. MADDIN and T. MASUMOTO, *Mater. Sci. Eng.* **9** (1972) 153.
3. T. MURAT, H. KIMURA and T. MASUMOTO, *Scripta Met.* **10** (1976) 705.
4. J. LOGAN and M. F. ASHBY, *Acta Met.* **22** (1974) 1074.
5. T. D. HADNAGY, D. J. KRENITSKY, D. G. AST and C. Y. LI, *Scripta Met.* **12** (1978) 45.
6. C. D. GRAHAM Jr, T. EGAMI, R. S. WILLIAMS and Y. TAKEI, Magnetism and Magnetic Materials, AIP Conference Proc. #29 (1975) edited by J. J. Becker, G. H. Lander and J. J. Rhyne (American Institute of Physics, New York, 1976) p. 218.
7. L. A. DAVIS, R. RAY, C. P. CHOU and R. C. O'HANDLEY, *Scripta Met.* **10** (1976) 541.
8. F. SPAEPEN, *Acta Met* **25** (1977) 407.
9. F. E. LUBORSKY, *Mater. Sci. Eng.* **28** (1977) 139.

Received 8 February and accepted 19 May 1978.